Optimization of sandwich plates with variable stiffness composite faces: free vibration and buckling behaviour

Daniel José Da Silva Fonseca
daniel.s.fonseca@tecnico.ulisboa.pt

Instituto Superior Técnico, Universidade de Lisboa, Portugal

December 2022

Abstract

Variable stiffness composite sandwich structures combine low density characteristics, provided by the core, with an immense potential of structural performance improvement due to the extended design space in comparison with traditional sandwich. These properties make variable stiffness sandwich structures very appealing for industries such as aerospace. In this work, the structures used possess face sheets that follow a linear fiber orientation law. Prior to the optimization phase, a study regarding the structural behaviour of these structures is made, primarly in terms of vibration and buckling. More concretely, the objective is to identify trends and possible correlations between the performance evolution and the laminas parameters (T_0 and T_1), as well as the impact of the core stiffness on the results. Possible onset of instabilities caused by face sheets with steered fibers is also investigated. Afterwards, an optimization process is made, resorting to *Matlab* genetic algorithm, combined with the structural analysis performed on *Abaqus*, using *Python* scripts. This process consists in four different uniobjective optimizations: free vibration, buckling in x and y directions and shear buckling. A plate with $1 \times 1\ m^2$, thickness of core of 16 mm and thickness of face sheet of 2 mm, being each face sheet composed of four laminas, is subjected to the optimization processes. It was concluded that, in the vast majority of optimization cases tested, VSS have a better structural performance than CSS. For example, the performance improvement achieved by VSS over CSS, in buckling in y direction, for CCCC boundary conditions, ascended to 67%.

Keywords: Variable Stiffness Sandwich, Local Instabilities, Genetic Algorithm, Natural Frequencies, Critical Buckling Load

1. Introduction

Sandwich composite structures are widely used today in the aerospace industry. Its great capabilities such as high stiffness, predominantly provided by the face sheets, combined with its low density, due to its considerably low density core, makes this type of structure one of the most common structures used in an industry in which weight has a strong impact. Therefore, a lot of effort has been put recently in the study of such structures in order to further improve its structural strengths. To this extent, variable stiffness sandwich (VSS) structures emerge as an alternative to the traditional constant stiffness sandwich (CSS) structures. Such terminology derives essentially from the nature of its face sheets, that consists of layers of fibers with variable spatial orientation. This particularity allows for an expansion of the design space. Although the main portion of research related to this topic concerns variable stiffness composite laminates, there are some studies regarding variable stiffness composite sandwich structures, although rarer. Therefore, this work intends to increase the available information and research concerning variable stiffness composite sandwich structures. Main objectives of this work comprise the structural study of the behaviour of variable stiffness sandwich, namely in vibration and buckling, and then exploring the capabilities of optimization algorithms to find the best solutions in such design space.

Tornabene et al. [1] conducts a vibration analysis over foam core variable stiffness composite sandwiches by employing a combined structural theory. This theory consists of an equivalent single layer approach based on the Carrera Unified Formulation. Moreover, in this work, to enhance and enrich the model, it is also added the Murakami's function to capture some particular effects related to soft core sandwich structures, with the vibration problem being solved numerically through the Generalized Differential Quadrature method. For more details on the theories and methods cited, see Tornabene et al. [1]. In what concerns curvilinear fiber orientation definition, in this work, different functions are used,

including the sine-wave, exponential and power-law distributions. It was concluded that the use of variable stiffness laminates as face sheets of sandwich structures can indeed vary quite significantly the vibration response and that there is room for further exploration of the capabilities of this type of structure.

A variable kinematic model is adopted by Vescovini and Dozio [2] to study the structural performance of variable stiffness laminated (VSL) plates and variable stiffness sandwich structures. Two types of fiber orientation laws are used: fiber orientation angle varying along x and fiber orientation angle varying along y. In either case, the linear fiber orientation law is used. In terms of sandwich materials, this work makes use of a sandwich structure with a low density and a high density core subjected to multiple boundary conditions. The results obtained using the proposed model are compared with other literature data and it is concluded that the model presented a good accuracy.

Loja et al. [3] studied and optimized the structural behaviour of laminated plates in vibration (also in statics and buckling). To this end, a first order shear deformation theory is used coupled with an adaptive hybrid optimization approach. The fiber paths are defined through a linear fiber orientation law in the study of three-ply laminates. In what relates to the vibration response, in this work, it is concluded that, for simply supported boundary conditions, the optimal fundamental frequency can be designed to be 5.61% higher than traditional constant stiffness laminates.

Some of the previous mentioned works, besides vibration analysis, also present buckling results. Vescovini and Dozio [2] is one of those cases, both in terms of VSL and VSS. In this topic, before a parametric study is done, a preliminary analysis is made to comprehend how the failure modes, namely local core crushing mechanisms, emerge with the combined effect of steered fibers on thick variable stiffness sandwich. Furthermore, this type of behaviour is magnified by the fiber steering component of VSS which worsens the buckling performance. Regarding the theories studied in this work, it is concluded that the layerwise theory, derived from the variable-kinematic approach, using Carrera's Unified Formulation and the Ritz method, is indeed necessary when analysing a sandwich with low density and shear stiffness core and that equivalent layer theories become inaccurate in these cases.

Coburn and Weaver [4] use a piecewise linear method for the fiber orientation law, with the sandwich panel being modelled as a Mindlin-Reissner two-dimensional plate, which accounts for transverse shear flexibility. In this work, the Ritz method is used to formulate the eigenvalue and eigenvector problems that model the buckling behaviour. In addition, a parametric study is performed by varying the parameters that govern the fiber orientation law. It was concluded that local instabilities occur more often in VSS when the sandwich core is of low density, which can make the buckling perfomance of VSS worse than classical sandwich.

Chen et al. [5] implemented a new method based on a modified extended high-order sandwich plate theory coupled with a Rayleigh-Ritz procedure to formulate the equations than govern the buckling problem in VSS. The theory converged to the same values of case studies available in literature and it is also concluded that VSS can improve buckling performance. However, for some cases such as certain fiber orientation laws or core density, there is an onset of different instabilities that cause this performance to greatly decrease.

2. Background

2.1. Variable Stiffness Sandwich - Fiber Orientation Law

The fiber path definition is expressed in a mathematical equation where θ is the fiber orientation in a given location. In the literature, there are a lot of options in what respects this definition.

In this work the fiber orientation is defined by a linear function. The reason to adopt such definition herein is not only its ease of implementation given its simplicity, but also the fact that it is the most commonly used definition in the literature, compared to other alternatives. Another advantage of using this definition concerns the optimization task, which benefits from having a lower number of design variables than other definitions. The general linear formulation starts with a value of T_0 from a reference point A, which is the center of the plate, changes along an axis x' (with origin in A), that is rotated of an angle ϕ from the standard coordinate x axis (horizontal axis), and finally reaches the final fiber angle value T_1 at $x' = d$, being d the distance from the reference point A [6]. The value of ϕ is taken as being 0 in this work.

In this work, the linear variation definition along the x' direction, that is, where the orientation θ depends only on the x' coordinate, is used. This definition is mathematically expressed in equation 1.

$$\theta(x') = (T_1 - T_0)\frac{|x'|}{a/2} + T_0 \tag{1}$$

In terms of notation, a variable stiffness lamina is represented by $<T_0, T_1>$, where T_0 is the fiber angle at the center of the lamina and T_1 the fiber angle at $x' = a/2$, where a is the length of the plate in the x' direction.

2.2. Curvature Constraint

There are currently two main techniques to implement a given path orientation definition: the shifted method and the parallel method. In the shifted method, the reference path is simply copied along a direction, in a translation movement. This allows for greater feasible designs, a greater stiffness variation when compared to the parallel method and makes the implementation of curvature constraints simpler. The main disadvantages of this method are the possible formation of gaps and overlaps, which in turn cause a thickness variation of the laminate. Continuous tow shearing (CTS) is assumed to be the manufacturing process used, thus avoiding the formation of gaps and overlaps which often originate from the Automated Fiber Placement (AFP) and in the shifted method.

Manipulation of the traditional curvature formula for a single variable function gives rise to the curvature constraint function used in the optimization process, given by equation 2:

$$K = \frac{2(T_1 - T_0)}{a} \cos\left((T_1 - T_0)\frac{|x'|}{a/2} + T_0\right) \quad (2)$$

In the literature, there are a multitude of values assigned to the curvature constraint. Some authors use 3.28 m^{-1} for the maximum allowable curvature. Furthermore, Kim et al. [7] reports that the curved paths used in the CTS process show a curvature 10 times bigger than the typical curvature exhibited by paths produced with the AFP process. Nonetheless, most values of curvature constraint available in literature are associated with the AFP process. Due to the lack of information concerning curvature values for CTS process, even though it allows the production of high curvature paths, in this work the value of $3.28m^{-1}$ is used in optimization process, as in [8, 9].

3. Stuctural Behaviour of Variable Stiffness Sandwich

3.1. Model Implementation and Validation

The finite element commercial software *Abaqus* is used to perform structural analysis. To achieve a compromise between the computational cost and the accuracy of both the structure modelling and the results, a mixed model is used, where the core is modelled with 3D elements to account for its high thickness and transverse flexibility and the face sheets are modelled with 2D shell elements, due to its low thickness and flexibility.

The model creation is done using *Python* scripts. The fiber orientation law is implemented through angle variation of the local coordinate system of each set of elements in the x direction (since, in this work, θ only varies according to x). So, at each element, the x coordinate of the centroid is calculated and the angle θ of the element in question is computed based on its centroid, being the angle constant in that element.

A model validation analysis is made involving VSS to assure that the structural behaviour of the model in both vibration and buckling reproduces valid results and in accordance with the available literature information. Results, presented in tables 1 and 2, are in line with the literature, with very acceptable deviations of around 1% or lower. A mesh consisted of 40×40 xy elements and 2 elements in the thickness of the core is used.

Table 1: Model validation with variable stiffness sandwich structures in vibration, in terms of non-dimensional fundamental frequency $\overline{\omega} = 2\pi f a^2 t^{-1}\sqrt{\frac{\rho^{face}}{E_y^{face}}}$. Face sheet configuration: [<0,45>, <-45,-60>, <0,45>].

Core material	b/h	ED2 [1]	ED4 [1]	LD1 [1]	LD2 [1]	Present model	Deviation, % (LD2)
Aluminium honeycomb [1]	10	3.682	3.361	3.311	3.309	3.296	0.390
	50	4.100	4.042	4.030	4.030	4.025	0.130
	100	4.143	4.114	4.108	4.108	4.098	0.250

Table 2: Model validation with variable stiffness sandwich structures in buckling ($b/h = 50$), in terms of nondimensional uniaxial x critical buckling force, $\overline{N}_x = \frac{N_x a^2}{E_x^{face} t^3}$.

Core material	Face sheet configuration	ED2 [2]	ED4 [2]	LD1 [2]	LD2 [2]	Present model	Deviation, % (LD2)
H Core (table 6)	[<0,30>, <0,-30>]	1.643	1.462	1.425	1.425	1.411	0.971
	[<0,60>, <0,-60>]	1.698	1.648	1.638	1.637	1.621	1.011
L Core (table 6)	[<0,30>, <0,-30>]	1.516	1.365	1.332	1.332	1.315	1.281
	[<0,60>, <0,-60>]	1.597	1.548	1.539	1.538	1.518	1.254

3.2. Core Stiffness Influence Study

One of the studies that is made in this work concerns the analysis of the relationship between the stiffness of the core and the results obtained, namely the possibility of the onset of particular failure modes. To this extent, isotropic and orthotropic cores are used. In order to conclude about the effect of the variation of core's stiffness on the results, this study begins with a particular core material and, afterwards, alters its properties to successively create new materials with progressively lower stiffness, both in the isotropic and orthotropic cases. The reference material (the first core of the isotropic table and the last core on the orthotropic table) for the isotropic case is a standard aluminium alloy [10] while for the orthotropic case the reference is an aluminium honeycomb [1]. The materials used are presented in tables 3, 4 and 5. All clamped boundary conditions (CCCC) are used and, in the buckling case, a normal compression force of 100 kN is used. Each face sheet has one lamina. Configurations with $T_0 = 0°$, $T_0 = 45°$ and $T_0 = 90°$ are used in this first study.

Table 3: Properties of the face sheet material used in the optimization processes [2].

	E_{11} (MPa)	E_{22} (MPa)	E_{33} (MPa)	ν_{12}	ν_{13}	ν_{23}	G_{12} (MPa)	G_{13} (MPa)	G_{23} (MPa)	ρ (kg/m^3)
CFRP	173000	7200	7200	0.29	0.29	0.29	3760	3760	3760	1540

Table 4: Orthotropic core materials used ($\rho = 72\ kg/m^3$).

Core material	E_{11} (MPa)	E_{22} (MPa)	E_{33} (MPa)	ν_{12}	ν_{13}	ν_{23}	G_{12} (MPa)	G_{13} (MPa)	G_{23} (MPa)
Core A	4400	4400	1536	0.99	0.0000864	0.0000864	27000	36900	22200
Core B	4400	4400	1536	0.99	0.0000864	0.0000864	2700	3690	2220
Core C	0.44	0.44	1536	0.99	0.0000864	0.0000864	2700	3690	2220
Core D [1]	0.44	0.44	1536	0.99	0.0000864	0.0000864	0.27	369	222

Table 5: Isotropic core materials used ($\rho = 2700\ kg/m^3$).

Core material	E (MPa)	ν
Core E [10]	70000	0.33
Core F	700	0.33
Core G	7	0.33
Core H	0.7	0.33

A particular aspect regarding the mode shape results is the onset, in some scenarios, of local failure modes or a coexistence of local and global instabilities. In both vibration and x buckling analysis, the local instability phenomenon is not present with this specific orientation law, for the set of configurations tested. However, for y buckling there are some configurations in which local instabilities occur. This phenomenon tends to occur in sandwich structures with specifically softer isotropic or orthotropic cores. In the latter, these instabilities are exacerbated and take a more irregular shape than in soft isotropic cores.

Figure 1 presents the mode shapes, in y buckling, regarding the isotropic core G with configurations $<0, 70>$, $<0, 80>$ and $<0, 90>$. It is possible to see that, in configuration $<0, 70>$, there is a coexistence of the traditional global mode with the presence of local instabilities, which progressively become the dominating mode as T_1 increases towards 90° (for $T_0 = 0°$, in this case). These failure modes are not transversal to all VSS, however. Configurations with high curvature exacerbate this phenomenon, as demonstrated by the degree of dominance of such modes over global modes as T_1 increases (i.e. curvature increases) for $T_0 = 0°$.

Therefore, it is possible to conclude that, although VSS can indeed bring benefits in terms of structural performance, careful thought must be taken in its design in order to conceive a structure that does not contribute to the earlier onset of such local failure modes with its drastic performance consequences. This type of failures are more often seen in y buckling, for the orientation law used and in the presence of softer cores.

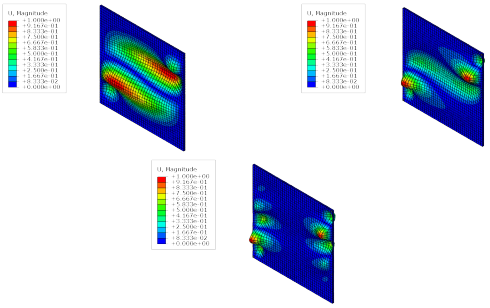

Figure 1: Mode shapes for configurations $<0, 70>$ (upper left), $<0, 80>$ (upper right) and $<0, 90>$ (lower center) with core G.

3.3. Low Stiffness Core Variable Stiffness Sandwich Study

This section consists on an in-depth investigation of the structural behaviour of VSS with low stiffness core. For antisymmetric face sheets configurations, the plots present the pair $<T_0, T_1>$ for the first lamina. The material used for the face sheets is the same as the previous study (CFRP), while the core's material is an aluminium honeycomb (core D, table 4).

Regarding the free vibration analysis, the first conclusion is that this type of analysis is less sensitive in what concerns the effects of low stiffness cores and variable stiffness face sheets on the onset of local failure modes. Indeed all fundamental modes observed are of global type.

In what concerns the symmetric face sheet configurations results, it is possible to observe that for boundary conditions such as CCCC, CCCF, CCFF, CFFF, CCSC or CCSS the general trend is that, with the increase of T_1 for a given value of T_0, the fundamental frequency decreases. The overview of the symmetric face sheets results (figure 2) allows to conclude that CSS tend to have a better performance than VSS, for the sets of configurations tested, in the majority of the boundary conditions.

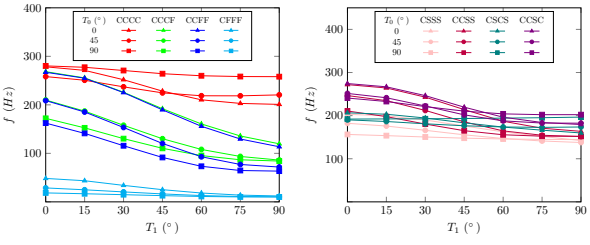

Figure 2: Fundamental frequency $f\ (Hz)$ evolution with T_0 and T_1 in multiple boundary conditions.

The general trend conclusions made for the symmetric cases are also applicable in the antisymmetric cases in what concerns the fundamental frequency evolution with T_1, for a given T_0, in the

different boundary conditions.

The results obtained related to uniaxial x buckling of both CSS and VSS with symmetrical face sheet configuration (figure 3) show that, for scenarios where at least one of the x edges ($x = 0$ or $x = a$) is clamped and remaining boundaries are either free or clamped, the CSS symmetrical configuration $<0, 0>$ has the best x buckling performance, as shown by the left plot of figure 3. In these same cases, besides this trend, there is also another visible pattern: for a given T_0, the increase of T_1, generally, decreases the buckling performance of the structure.

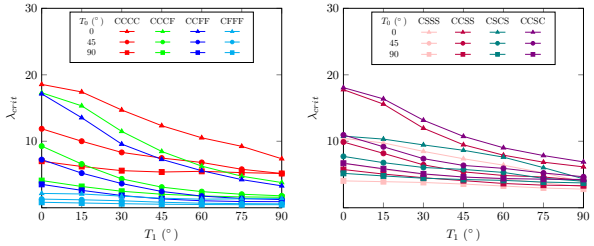

Figure 3: Uniaxial x buckling critical load factor (λ_{crit}) evolution with T_0 and T_1 in multiple boundary conditions.

The results for antisymmetric face sheet configurations dictate that the behaviour of these structures, unlike the vibration case, have a quite significantly different response in comparison with the symmetric counterparts. An example of the previously stated is visible in the CCCC test: while, in the symmetric configurations, for all T_0 there is rapid decrease of performance with the increase of T_1, in the antisymmetric configurations the decrease of performance is very slow and, in the case of $T_0 = 45°$, it actually increases until it reaches the peak of critical buckling load at $<45, 30>$, after which decreases, as seen in the left plot of figure 4.

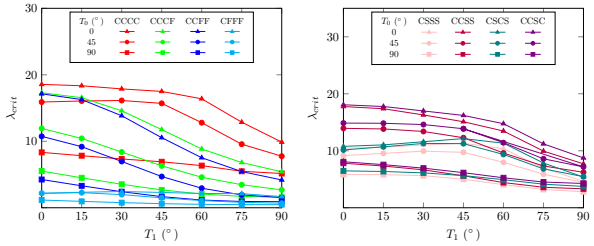

Figure 4: Uniaxial x buckling critical load factor (λ_{crit}) evolution (antisymmetric facesheet configuration) with T_0 and T_1 in multiple boundary conditions.

The uniaxial y buckling analysis of symmetrical face sheet configurations reveals different conclusions regarding the evolution of buckling performance in comparison with x buckling. For instance, in the left plot of figure 5, when CCCC conditions are applied, it is possible to observe that the VSS $<45, 90>$ configuration has better performance than other configurations, including CSS. For the same boundary conditions, the uniaxial x buckling has a CSS configuration as its best configuration, which allows to conclude that, not only the performance depends on the boundary conditions applied and whether CSS or VSS are used, but also in which direction the buckling analysis is made. Furthermore, for this boundary condition, the performance increases, for a given T_0, with the increase of T_1, whereas for the remaining conditions of the same plot (CCCF, CCFF and CFFF) the performance stagnates at a certain value or decreases slowly.

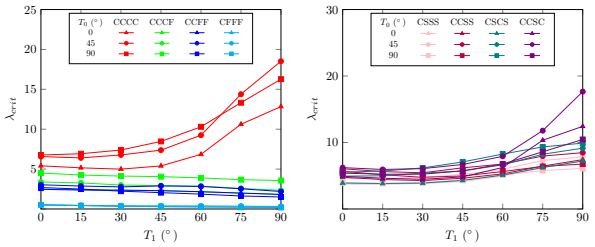

Figure 5: Uniaxial y buckling critical load factor (λ_{crit}) evolution with T_0 and T_1 in multiple boundary conditions.

In contrast to the results obtained in uniaxial x buckling, antisymmetric face sheet configurations do not always perform better than the symmetrical cases, having, in some scenarios, worse performance. In figure 6, there are a multitude of curves in the different plots that have a similar behaviour: the buckling performance increases until $T_1 = 45°$, then decreases until $T_1 = 75°$ and once again increases until $T_1 = 90°$. The former is verified, for example, in CCCC and CCSC conditions for configurations with $T_0 = 45°$. So, although there are plenty of curves with the same increasing performance behaviour with increasing T_1 as it was detected in the symmetrical cases, the introduction of the antisymmetric lamina produced a less straightforward curve evolution for the critical buckling load factor for some boundary conditions.

4. Optimization Problem Formulation

The objective of the optimization processes of the present work is to maximize the fundamental frequency, in the vibration case, and to maximize the critical buckling load, in the buckling case. To this extent, *Matlab* genetic algorithm is used, coupled with *Python* scripts used for the structural analysis in *Abaqus*. A plate with $1 \times 1\ m^2$ is used, being the sandwich structure composed of a core with thickness $t_c = 16\ mm$ and two face sheets which are

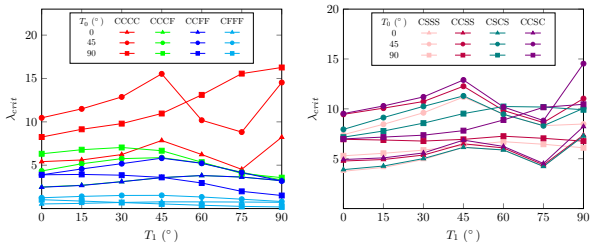

Figure 6: Uniaxial y buckling critical load factor (λ_{crit}) evolution (antisymmetric facesheet configuration) with T_0 and T_1 in multiple boundary conditions.

composite laminates composed of 4 laminas (i.e., 8 design variables overall), in a total face sheet thickness of $t_f = 2\ mm$.

The optimization problem is formulated in the following way:

$$\begin{aligned} &\text{maximize} \quad f(\boldsymbol{x}) \\ &\text{with} \quad \boldsymbol{x} \in \mathbb{Z} \\ &\text{subjected to} \quad g_i(\boldsymbol{x}) \geq 0, \quad i = 1, ..., N_L \end{aligned} \tag{3}$$

where $\boldsymbol{x}$ is the vector containing the decision variables $[<T_0, T_1>]_i$ for each lamina i, in the case of curvilinear fibers, and $[T_0]_i$, in the case of straight fibers, $f(\boldsymbol{x})$ is the objective function (fundamental frequency in vibration and critical buckling load in buckling) and $g_i(\boldsymbol{x})$ are the nonlinear constraints, being N_L the number of laminas.

For curvilinear fibers, since the orientation law chosen is defined by a linear function, there are two decision variables per lamina. In this work, the sandwich structure is symmetric, that is, the composite laminates (top face sheet and bottom face sheet) are symmetric to one another about the midplane of the sandwich core but the face sheets themselves are not necessarily symmetric. Thus, the total amount of decision variables is eight. Moreover, it is assumed that the decision variables only take integer values and not the general case of being a real number. That is due to the fact that the variation of the decision variables (T_0 and T_1 for each lamina) in the decimal places would not differ significantly from their nearest integer counterpart. Furthermore, the inclusion of the possibility of x taking on real values would cause a slower convergence. The non linear constraints, $g_i(\boldsymbol{x})$, concern, in this case, the curvature constraint given by equation 2.

The properties of the materials used in the optimization processes of both core and face sheets are summarized in tables 3 and 6. For the cores, two types of aluminium honeycomb material are used: one of lower density and stiffness denoted aluminium honeycomb of low stiffness (AH-L) and one of higher density and stiffness denoted aluminium honeycomb of high stiffness (AH-H). In what concerns the face sheets, a carbon fiber reinforced plastic (CFRP) was used.

Table 6: Properties of the cores used in the optimization processes [2].

	E_{11} (MPa)	E_{22} (MPa)	E_{33} (MPa)	ν_{12}	ν_{13}	ν_{23}	G_{12} (MPa)	G_{13} (MPa)	G_{23} (MPa)	ρ (kg/m^3)
AH-H	12	12	4608	0.99	7.74e-4	7.76e-4	7	1108	664	192
AH-L	0.44	0.44	1536	0.99	8.64e-5	8.64e-5	0.27	369	222	72

In terms of boundary conditions, simply supported in all side faces and edges (SSSS) as well as clamped boundary conditions (CCCC) are applied.

5. Optimization Results

5.1. Aluminium Honeycomb Core of High Stiffness Results

Optimal CSS and VSS face sheet configuration, with a sandwich core made of AH-H material, and respective optimal result, for the four types of structural analysis made, subjected to CCCC boundary conditions, are presented in tables 7 and 8.

Regarding the vibration result, the only similarity to the optimal CSS result is that the optimal VSS result has a face sheet configuration that includes an almost constant stiffness lamina aligned closely with the x direction (lamina 2 with $T_0 = -9$, $T_1 = -4$), as it occurred in the CSS (3 laminas aligned with the x' direction, $T_0 = T_1 = 0°$). The remaining laminas of the optimal VSS reveal the higher design flexibility of this type of sandwich structure over CSS, with all three laminas being aligned, at the half-length of the structure ($x = a/2 = 0.5m$), with the y direction ($T_0 = 90°$ or $T_0 = -90°$) and, at $x = 0m$ and $x = a = 1m$, closely aligned with the x direction ($(T_1)_1 = 0$, $(T_1)_3 = 2°$ and $(T_1)_4 = -3°$).

Buckling in the x direction result shows that the optimal VSS is achieved with lamina 1 being almost antisymmetric of lamina 2 and lamina 3 almost antisymmetric of lamina 4. However, the two first laminas have a completely different fiber path orientation evolution than the latter two. Laminas 1 and 2 fiber path begins with a $14°$ (or $-14°$) orientation at $x = 0$, therefore close to being aligned with the x' direction. On the other hand, laminas 3 and 4 fiber path initiates with an orientation close to a $45°$ (or $-45°$) angle, more noticeable in lamina 3 ($(T_1)_3 = 41°$ while $(T_1)_4 = -33°$), and then evolves to an orientation, at $x = a/2$, practically aligned with the x direction ($(T_0)_3 = -2°$ and $(T_0)_4 = 1°$). This VSS configuration provides a critical buckling load factor, λ_{crit}, 27.073% higher than the optimal CSS configuration.

In relation to the buckling in the y direction result, the use of VSS reveals to be even more beneficial, in a performance point of view, than in buckling in the x direction, since the optimal VSS con-

figuration achieves a 67.304% critical buckling load factor improvement in comparison to the optimal result obtained with CSS. The optimal VSS result is achieved with a face sheet configuration composed of two (out of four) virtually equal laminas (laminas 1 and 4), with an orientation, at $x = 0$ and $x = a$, closely aligned with the y' direction ($(T_1)_1 = -84°$ and $(T_1)_4 = -83°$), then developing towards to an orientation direction closer to the x' direction than the y direction ($(T_0)_1 = -30°$ and $(T_0)_4 = -32°$), at $x = a/2$. Lamina 2 is practically an antisymmetric configuration of the two previous mentioned laminas, being only lamina 3 the "outsider" with $T_0 = -57°$ and $T_1 = -6°$ values significantly different from the remaining laminas.

An interesting observation is that optimal CSS critical buckling load factor values for buckling in x and y direction does not vary much: 22.129 in buckling in x direction and 21.394 in buckling in y direction (a difference of only 3.436% taking the smaller value as reference). On the other hand, the same conclusion does not apply to VSS results, with the critical buckling load factor in y direction being significantly higher than the one verified in the x direction (35.793 and 28.120, respectively, a difference of 27.289% taking the smaller value as reference). This difference as well as the higher performance difference between optimal VSS and CSS configuration verified in buckling in y direction can be explained by the fiber orientation law used. Indeed, in the buckling in y direction there is a concentration, namely in laminas 1,2 and 4, of load direction oriented fibers (that is, fibers oriented in the load direction, which is, in this case, the y direction) in small regions in the extremities of the sandwich structure (near $x = 0$ and $x = a$). This leads to a higher structural stiffness since multiple fibers are accumulated in that concentrated region, oriented in the load direction, magnifying the stiffness effect and, therefore, increasing quite significantly the critical buckling load factor.

In shear buckling, optimal VSS can, as well, improve the structural performance, in this case up to 47.192% higher critical shear buckling load factor than optimal CSS, in CCCC boundary conditions and with AH-H core. This performance improvement is achieved with a VSS configuration composed of one almost straight lamina (lamina 1) combined with two antisymmetric laminas (laminas 2 and 3) and a final lamina that, although being almost straight, it has a small steering effect that allows for some fiber concentration at $x = 0$ and $x = a$, as seen in figure 10. The optimal VSS configuration in shear buckling is characterized, namely, by a less pronounced curvature in all laminas, contrasting with some optimal configurations in other structural analysis.

Table 7: Optimization results for vibration, buckling x, buckling y and shear buckling for CCCC boundary conditions with AH-H material as core and constant stiffness composite face sheets.

Aluminium honeycomb core of high stiffness (AH-H)					
Structural Analysis	Boundary conditions				
	CCCC				
	Optimal face sheet configuration				Optimal result
	$< T_0, T_1 >_1$	$< T_0, T_1 >_2$	$< T_0, T_1 >_3$	$< T_0, T_1 >_4$	
Vibration (f in Hz)	$< 0, 0 >$	$< 0, 0 >$	$< 0, 0 >$	$< -90, -90 >$	277.804
Buckling x (λ_{crit})	$< -58, -58 >$	$< 11, 11 >$	$< 10, 10 >$	$< 6, 6 >$	22.129
Buckling y (λ_{crit})	$< 89, 89 >$	$< 89, 89 >$	$< -2, -2 >$	$< 88, 88 >$	21.394
Shear buckling (λ_{crit})	$< 0, 0 >$	$< 36, 36 >$	$< 0, 0 >$	$< 88, 88 >$	39.587

Table 8: Optimization results for vibration, buckling x, buckling y and shear buckling for CCCC boundary conditions with AH-H material as core and variable stiffness composite face sheets.

Aluminium honeycomb core of high stiffness (AH-H)					
Structural Analysis	Boundary conditions				
	CCCC				
	Optimal face sheet configuration				Optimal result
	$< T_0, T_1 >_1$	$< T_0, T_1 >_2$	$< T_0, T_1 >_3$	$< T_0, T_1 >_4$	
Vibration (f in Hz)	$< 90, 0 >$	$< -9, -4 >$	$< -90, 2 >$	$< 90, -3 >$	308.592
Buckling x (λ_{crit})	$< -79, -14 >$	$< 81, 14 >$	$< -2, 41 >$	$< 1, -33 >$	28.120
Buckling y (λ_{crit})	$< -30, -84 >$	$< 28, 74 >$	$< -57, -6 >$	$< -32, -83 >$	35.793
Shear buckling (λ_{crit})	$< -8, -13 >$	$< 50, 15 >$	$< -51, -17 >$	$< 73, 84 >$	58.269

Regarding CSS and VSS optimization with SSSS boundary conditions, in a sandwich structure with AH-H as core, tables 9 and 10 present the results for vibration, buckling in x direction, buckling in y direction and shear buckling. Under SSSS boundary conditions, sandwich structures become more flexible, and therefore, less stiffer, leading to lower optimal values of critical buckling load factors and fundamental frequency in comparison to CCCC boundary conditions results.

The vibration result shows that, unlike the CCCC boundary condition case, the difference in fundamental frequency performance between optimal VSS and CSS configurations is virtually negligible. Indeed the difference is only of 0.01% which allows to infere that, realistically, the introduction of steered fibers in sandwich structure's face sheets does not improve the verified performance in CSS.

Concerning the buckling in x direction result, the performance improvement of the optimal VSS over CSS, albeit not being equally as high as occurred under CCCC boundary conditions, ascends to 20% in terms of critical buckling load factor. To achieve such performance, optimal VSS configuration includes, in its composition, two antisymmetric laminas (lamina 1 and 2) and two symmetric laminas (lamina 3 and 4), a peculiarity first seen in all of the

optimal face sheet configurations until here analysed. The two antisymmetric laminas are characterized by a smooth fiber path orientation, with a less pronounced curvature than in, for example, the analogous result in CCCC conditions.

In relation to the buckling y result, the performance improvement of VSS is, once again, smaller than in CCCC conditions, being, nonetheless, significant. The difference between VSS and CSS ascends to 24.5% in terms of critical buckling load factor. Although the performance improvement in buckling in y direction is still higher than the one verified in buckling in x direction, due to the reasons already mentioned in the CCCC boundary conditions results analysis, it appears that the change from CCCC to SSSS conditions leads to a mitigation of the magnification verified in the previous boundary condition scenario.

Table 9: Optimization results for vibration, buckling x and buckling y for SSSS boundary conditions with AH-H material as core and constant stiffness composite face sheets.

Aluminium honeycomb core of high stiffness (AH-H)					
Structural Analysis	Boundary conditions				
	SSSS				
	Optimal face sheet configuration				Optimal result
	$< T_0, T_1 >_1$	$< T_0, T_1 >_2$	$< T_0, T_1 >_3$	$< T_0, T_1 >_4$	
Vibration (f in Hz)	$< 44, 44 >$	$< -44, -44 >$	$< 47, 47 >$	$< -43, -43 >$	165.282
Buckling x (λ_{crit})	$< 44, 44 >$	$< 44, 44 >$	$< -44, -44 >$	$< -43, -43 >$	9.947
Buckling y (λ_{crit})	$< -41, -41 >$	$< 46, 46 >$	$< 45, 45 >$	$< -46, -46 >$	10.094

Table 10: Optimization results for vibration, buckling x and buckling y for SSSS boundary conditions with AH-H material as core and variable stiffness composite face sheets.

Aluminium honeycomb core of high stiffness (AH-H)					
Structural Analysis	Boundary conditions				
	SSSS				
	Optimal face sheet configuration				Optimal result
	$< T_0, T_1 >_1$	$< T_0, T_1 >_2$	$< T_0, T_1 >_3$	$< T_0, T_1 >_4$	
Vibration (f in Hz)	$< 44, 45 >$	$< -44, -45 >$	$< -46, -44 >$	$< 46, 43 >$	165.499
Buckling x (λ_{crit})	$< -69, -44 >$	$< 64, 45 >$	$< -2, 55 >$	$< -2, -53 >$	11.937
Buckling y (λ_{crit})	$< 31, 44 >$	$< -40, -46 >$	$< 25, 73 >$	$< -35, -69 >$	12.568

5.2. Aluminium Honeycomb Core of Low Stiffness Results

Optimization results of CSS with AH-L as core and subjected to CCCC boundary conditions are presented in table 11. The values achieved for optimal results in the different structural analysis show that, in comparison to CSS with AH-H as core subjected to the same CCCC boundary conditions, optimal fundamental frequency result with AH-L is higher while optimal critical buckling load factor in both buckling in x and buckling in y directions are lower. Indeed, the use of AH-L as core, in comparison to AH-H, leads to a decrease in both stiffness and density (ρ). The decrease in stiffness inevitably leads to the decrease observed in critical buckling load factors since the structure is less robust to cope with the buckling forces. The change in density is, probably, the main driver of the increase of performance verified in vibration, since lower density structures, typically, have higher fundamental frequencies, while higher density structures (as in the sandwich cases with AH-H), due to inertia reasons, tend to vibrate at lower frequencies.

Optimal VSS face sheet configuration, in vibration, for an AH-L sandwich core, is very similar to that obtained when using AH-H sandwich core. In fact, both optimal configurations try to take maximum advantage of curvature constraint, leading to configurations with highly steered fibers. This optimal VSS configuration achieves a fundamental frequency improvement of 7.795% over the optimal CSS configuration, in CCCC boundary conditions.

Regarding optimal results obtained in buckling in x direction, optimal VSS critical buckling load factor achieved with AH-L sandwich core is lower (19.218%) than the AH-H VSS case, due to its lower stiffness. The optimal VSS face sheet configuration has, in its composition, three virtually identical laminas (laminas 1,2 and 4), which start with a orientation value near the $-45°$ mark, at $x' = 0$, then progressively evolves to higher orientation values, reaching, at $x' = a/2$, a orientation closely aligned with the x direction ($(T_0)_1 = 16°$, $(T_0)_2 = 15°$, $(T_0)_4 = 12°$). The performance improvement proves that extremely low stiffness core penalize the performance improvement provided by optimal VSS configurations over CSS. This may be due to the fact that, in the presence of softer cores, there is a higher probability of local instabilities that decrease significantly VSS performance, while also narrowing the range of possible VSS that can outperform CSS.

The use of steered fibers in the structure, subjected to CCCC conditions, leads to an 55.301% critical y buckling load factor improvement over CSS. This improvement is, however, smaller than the one verified with AH-H. The lower stiffness of the AH-L core leads to, as it occurred in the buckling in x direction, a significantly lower optimal value for critical buckling load factor (27.743, which is 29.016% lower than the value obtained with optimal configuration with AH-H core). There is, nonetheless, more similarities, in what concerns the optimal face sheet configurations (in buckling in y direction) composition in each of the cores, than in the buckling in x direction. In both core cases, the optimal face sheet configuration has two almost

equal laminas (laminas 1 and 4 in both cases) with lamina 2 being an almost antisymmetric counterpart of the previous two.

The impact of the change from AH-H to AH-L and consequent decrease of stiffness is also noticeable in shear buckling result, with optimal VSS achieving a critical buckling load factor of 33.394, which represents a 41.763% decrease of the value obtained by optimal VSS with AH-H core. Furthermore, the core change also has a major impact in the performance improvement provided by optimal VSS. The performance achieved by optimal VSS is 6.103% higher than the one verified with optimal CSS. This improvement is drastically smaller than the one verified with optimal VSS over optimal CSS in the presence of an AH-H core.

Illustrative representations of the optimal VSS fiber paths in the various analysis, under CCCC conditions, are presented in figures 7, 8, 9, 10 11, 12, 13 and 14.

Table 11: Optimization CSS results for vibration, buckling x, buckling y and shear buckling for CCCC conditions with AH-L material as core.

Aluminium honeycomb core of low stiffness (AH-L)					
Structural Analysis	Boundary conditions				
	CCCC				
	Optimal face sheet configuration				Optimal result
	$< T_0, T_1 >_1$	$< T_0, T_1 >_2$	$< T_0, T_1 >_3$	$< T_0, T_1 >_4$	
Vibration (f in Hz)	$< 0, 0 >$	$< 0, 0 >$	$< 0, 0 >$	$< -90, -90 >$	289.259
Buckling x (λ_{crit})	$< 0, 0 >$	$< -90, -90 >$	$< 0, 0 >$	$< 0, 0 >$	19.198
Buckling y (λ_{crit})	$< 18, 18 >$	$< -24, -24 >$	$< 89, 89 >$	$< 89, 89 >$	17.864
Shear buckling (λ_{crit})	$< -15, -15 >$	$< 39, 39 >$	$< 42, 42 >$	$< -40, -40 >$	31.982

Table 12: Optimization VSS results for vibration, buckling x, buckling y and shear buckling for CCCC conditions with AH-L material as core.

Aluminium honeycomb core of low stiffness (AH-L)					
Structural Analysis	Boundary conditions				
	CCCC				
	Optimal face sheet configuration				Optimal result
	$< T_0, T_1 >_1$	$< T_0, T_1 >_2$	$< T_0, T_1 >_3$	$< T_0, T_1 >_4$	
Vibration (f in Hz)	$< 90, 0 >$	$< -5, -4 >$	$< -90, 1 >$	$< 90, 2 >$	311.808
Buckling x (λ_{crit})	$< 16, -38 >$	$< 15, -37 >$	$< 90, 42 >$	$< 12, -34 >$	23.587
Buckling y (λ_{crit})	$< 38, 83 >$	$< -48, -75 >$	$< -71, 0 >$	$< 42, 86 >$	27.743
Shear buckling (λ_{crit})	$< 26, -2 >$	$< -45, -1 >$	$< -54, -36 >$	$< 51, 31 >$	33.934

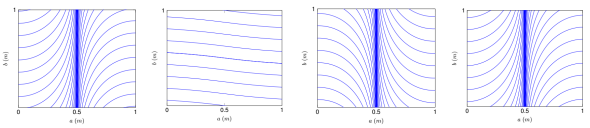

Figure 7: Fiber paths for optimal VSS in vibration with AH-H core and CCCC conditions.

Table 13: Optimization CSS results for vibration, buckling x and buckling y for SSSS conditions with AH-L material as core.

Aluminium honeycomb core of low stiffness (AH-L)					
Structural Analysis	Boundary conditions				
	SSSS				
	Optimal face sheet configuration				Optimal result
	$< T_0, T_1 >_1$	$< T_0, T_1 >_2$	$< T_0, T_1 >_3$	$< T_0, T_1 >_4$	
Vibration (f in Hz)	$< -37, -37 >$	$< 56, 56 >$	$< 47, 47 >$	$< -44, -44 >$	172.620
Buckling x (λ_{crit})	$< 43, 43 >$	$< 44, 44 >$	$< -44, -44 >$	$< -43, -43 >$	8.723
Buckling y (λ_{crit})	$< 50, 50 >$	$< -42, -42 >$	$< -44, -44 >$	$< 44, 44 >$	8.800

Table 14: Optimization VSS results for vibration, buckling x and buckling y for SSSS conditions with AH-L material as core.

Aluminium honeycomb core of low stiffness (AH-L)					
Structural Analysis	Boundary conditions				
	SSSS				
	Optimal face sheet configuration				Optimal result
	$< T_0, T_1 >_1$	$< T_0, T_1 >_2$	$< T_0, T_1 >_3$	$< T_0, T_1 >_4$	
Vibration (f in Hz)	$< -49, 40 >$	$< 46, 42 >$	$< -41, -46 >$	$< 41, 46 >$	173.829
Buckling x (λ_{crit})	$< -70, -45 >$	$< -10, 56 >$	$< 56, 46 >$	$< 2, -54 >$	10.322
Buckling y (λ_{crit})	$< -56, -19 >$	$< 8, 87 >$	$< 17, 59 >$	$< -49, -60 >$	10.866

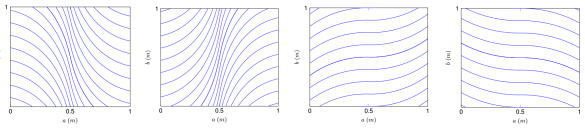

Figure 8: Fiber paths for optimal VSS in buckling in x with AH-H core and CCCC conditions.

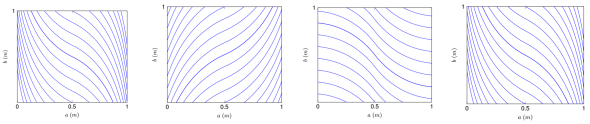

Figure 9: Fiber paths for optimal VSS in buckling in y with AH-H core and CCCC conditions.

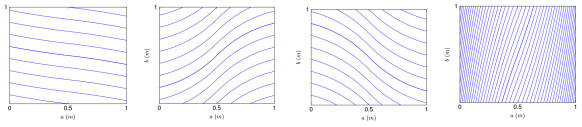

Figure 10: Fiber paths for optimal VSS in shear buckling with AH-H core.

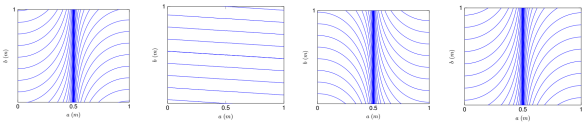

Figure 11: Fiber paths for optimal VSS in vibration with AH-L core and CCCC conditions.

6. Conclusions

The work done herein constitutes an elaborated foundation for the study and optimization of VSS.

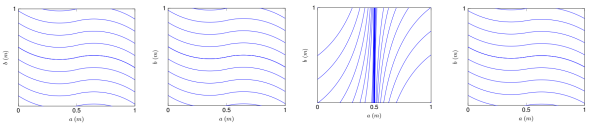

Figure 12: Fiber paths for optimal VSS in buckling in x with AH-L core and CCCC conditions.

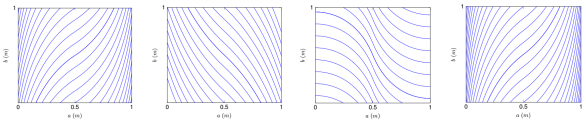

Figure 13: Fiber paths for optimal VSS in buckling in y with AH-L core and CCCC conditions.

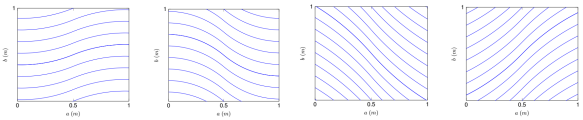

Figure 14: Fiber paths for optimal VSS in shear buckling with AH-L core.

An in-depth study of the structural behaviour of VSS, in comparison with CSS, prior to the optimization process, is done. In the presence of low density and stiffness sandwich cores, which constitute the majority of types of core used in aerospace, it was possible to identify some trends and performance evolution with parameter variation (T_0 and T_1) of VSS. The results obtained pointed in the direction that VSS were structurally superior to CSS configurations in multiple cases.

It was concluded that, in the vast majority of optimization cases tested, VSS have a better or a much better structural performance than CSS. For example, the performance improvement achieved by VSS over CSS, in buckling in y direction, for CCCC boundary conditions, ascended to 67%. The capability of steered fibers to provide for different stiffness characteristics in different regions of the structure reveals to be essential for the improvements verified. This is due to the fact that the same fiber can improve stiffness in different directions in different regions of the same lamina, unlike unsteered fibers which can only provide stiffness uniformly in one direction, across the entire length of the lamina.

Future studies following this work include, for example, the use of other fiber orientation laws which can be more accurate in certain scenarios or the use of other types of geometry , namely to comprehend how does the structural behaviour VSS change in the presence of curved surfaces in its geometry.

References

[1] F. Tornabene, N. Fantuzzi, and M. Bacciocchi. Foam core composite sandwich plates and shells with variable stiffness: Effect of the curvilinear fiber path on the modal response. *Journal of Sandwich Structures & Materials*, 21(1):320–365, 2019. doi: 10.1177/1099636217693623.

[2] R. Vescovini and L. Dozio. A variable-kinematic model for variable stiffness plates: Vibration and buckling analysis. *Composite Structures*, 142:15–26, 2016. doi: 10.1016/j.compstruct.2016.01.068.

[3] M. Loja, F. Marques, and A. Mota. Variable stiffness composites: Optimal design studies. *Journal of Composites Science*, 4:80, 2020. doi: 10.3390/jcs4020080.

[4] B. H. Coburn and P. M. Weaver. Buckling analysis, design and optimisation of variable-stiffness sandwich panels. *International Journal of Solids and Structures*, 96:217–228, 2016. doi: 10.1016/j.ijsolstr.2016.06.007.

[5] X. Chen, G. Nie, and Z. Wu. Global buckling and wrinkling of variable angle tow composite sandwich plates by a modified extended high-order sandwich plate theory. *Composite Structures*, 292:115639, 2022. doi: 10.1016/j.compstruct.2022.115639.

[6] Z. Gürdal, B. Tatting, and C. Wu. Variable stiffness composite panels: Effects of stiffness variation on the in-plane and buckling response. *Composites Part A: Applied Science and Manufacturing*, 39(5):911–922, 2008. doi: 10.1016/j.compositesa.2007.11.015.

[7] B. C. Kim, P. M. Weaver, and K. Potter. Manufacturing characteristics of the continuous tow shearing method for manufacturing of variable angle tow composites. *Composites Part A: Applied Science and Manufacturing*, 61:141–151, 2014. doi: 10.1016/j.compositesa.2014.02.019.

[8] H. Akhavan and P. Ribeiro. Natural modes of vibration of variable stiffness composite laminates with curvilinear fibers. *Composite Structures*, 93(11):3040–3047, 2011. doi: 10.1016/j.compstruct.2011.04.027.

[9] C. Waldhart. Analysis of tow-placed, variable-stiffness laminates. Master's thesis, Faculty of the Virginia Polytechnic Institute and State University, 1996.

[10] K. Foo, L. Seah, and G. Chai. Low-velocity impact failure of aluminium honeycomb sandwich panels. *Composite Structures*, 85(1):20–28, 2008. doi: 10.1016/j.compstruct.2007.10.016.